Pergamon

Geochimica et Cosmochimica Acta, Vol. 67, No. 1, pp. 153–169, 2003

0016-7037/03 $22.00 + .00

PII S0016-7037(02)01045-1

Dark inclusions in CO3 chondrites: New indicators of parent-body processes

DAISUKE ITOH and KAZUSHIGE TOMEOKA*

Department of Earth and Planetary Sciences, Faculty of Science, Kobe University, Nada, Kobe 657-8501, Japan

(*Received January* 24, 2002; *accepted in revised form July* 9, 2002)

Abstract—A petrographic and scanning electron microscopic study of the four CO3 chondrites Kainsaz, Ornans, Lancé, and Warrenton reveals for the first time that dark inclusions (DIs) occur in all the meteorites. DIs are mostly smaller in size than those reported from CV3 chondrites. They show evidence suggesting that they were formed by aqueous alteration and subsequent dehydration of a chondritic precursor and so probably have a formation history similar to that of DIs in CV3 chondrites. DIs in the CO3 chondrites consist mostly of fine-grained, Fe-rich olivine and can be divided into two types on the basis of texture. Type I DIs contain rounded, porous aggregates of fine grains in a fine-grained matrix and have textures suggesting that they are fragments of chondrule pseudomorphs. Veins filled with Fe-rich olivine are common in type I DIs, providing evidence that they experienced aqueous alteration on the parent body. Type II DIs lack rounded porous aggregates and have a matrix-like, featureless texture. Bulk chemical compositions of DIs and mineralogical characteristics of olivine grains in DIs suggest that these two types of DIs have a close genetic relationship.

The DIs are probably clasts that have undergone aqueous alteration and subsequent dehydration at a location different from the present location in the meteorites. The major element compositions, the mineralogy of metallic phases, and the widely dispersed nature of the DIs suggest that their precursor was CO chondrite material. The CO parent body has been commonly regarded to have been dry, homogeneous, and unprocessed. However, the DIs suggest that the CO parent body was a heterogeneous conglomerate consisting of water-bearing regions and water-free regions and that during asteroidal heating, the water-bearing regions were aqueously altered and subsequently dehydrated. Brecciation may also have been active in the parent body.

The DIs and the matrices are similarly affected by thermal metamorphism in their own host CO3 chondrites (petrologic subtypes 3.1 to 3.6), but the degree of the secondary processing (aqueous alteration and subsequent dehydration) of the DIs has no apparent correlation with the petrologic grades of the host chondrites. These observations suggest that the DIs had been incorporated into the host chondrites before the thermal metamorphism took place and that the secondary processes that affected the DIs largely occurred before the thermal metamorphism. *Copyright © 2003 Elsevier Science Ltd*

1. INTRODUCTION

CO and CV chondrites are two major chemical groups of carbonaceous chondrites that are both classified as petrologic type 3 and are generally similar in bulk chemical composition and mineralogy. An interesting contrast exists, however, in the abundance of dark inclusions (DIs). DIs are reportedly common in CV3 chondrites (e.g., Fruland et al., 1978; Johnson et al., 1990), whereas no DIs have been described from CO3 chondrites. This fact raises a fundamental question of whether DIs are unique to CV3 chondrites and do not really occur in CO3 chondrites. There is a growing consensus that DIs in CV3 chondrites serve as important indicators of the processes that occurred at or before the final assembly of the CV parent body. Therefore, we believe that the question raised above has implications regarding the formation history of CO3 chondrites as well as CV3 chondrites. This study was initiated to search for DIs in CO3 chondrites.

DIs in CV3 chondrites show a wide range of variation in texture; they contain various proportions of chondrules, porous aggregates of fine-grained olivine, and Ca-Al-rich inclusions (CAIs) in fine-grained matrices (e.g., Fruland et al., 1978; Johnson et al., 1990). Despite textural variations, DIs are similar in bulk chemical, oxygen isotopic, and noble gas isotopic composition to their host CV3 chondrites (Palme et al., 1989; Johnson et al., 1990; Bunch et al., 1980), which suggests a close genetic relationship between them. The origin of DIs has been a subject of extensive controversy for the past decade; the opinions have been mainly divided into the following two camps: DIs are (1) primary aggregates of condensates from the solar nebula (Kurat et al., 1989; Palme et al., 1989; Weisberg and Prinz, 1998) or (2) fragments of the CV parent body that were aqueously altered and subsequently dehydrated on the parent body (Kojima et al., 1993; Kojima and Tomeoka, 1996; Krot et al., 1997, 1998, 1999; Buchanan et al., 1997).

We performed an extensive survey of petrographic thin sections of the four non-Antarctic CO3 chondrites Kainsaz (petrologic grade 3.1), Ornans (3.3), Lancé (3.4), and Warrenton (3.6) and found a total of 101 inclusions that are dark and translucent in transmitted light. We initially discovered an exceptionally large DI (1.2 × 0.5 mm) in Ornans (see Fig. 1a), and a detailed study of it led us to find numerous inclusions having similar texture and mineralogy but much smaller sizes in all four chondrites. In this paper, we present the results of detailed petrographic and scanning electron microscope (SEM) observations of those DIs. Our goals were to determine whether DIs formed in the solar nebula or in the parent body and to determine differences, if any, in the formation processes of DIs in CO3 and in CV3 chondrites. The four CO3 chondrites range

* Author to whom correspondence should be addressed (tomeoka@kobe-u.ac.jp).

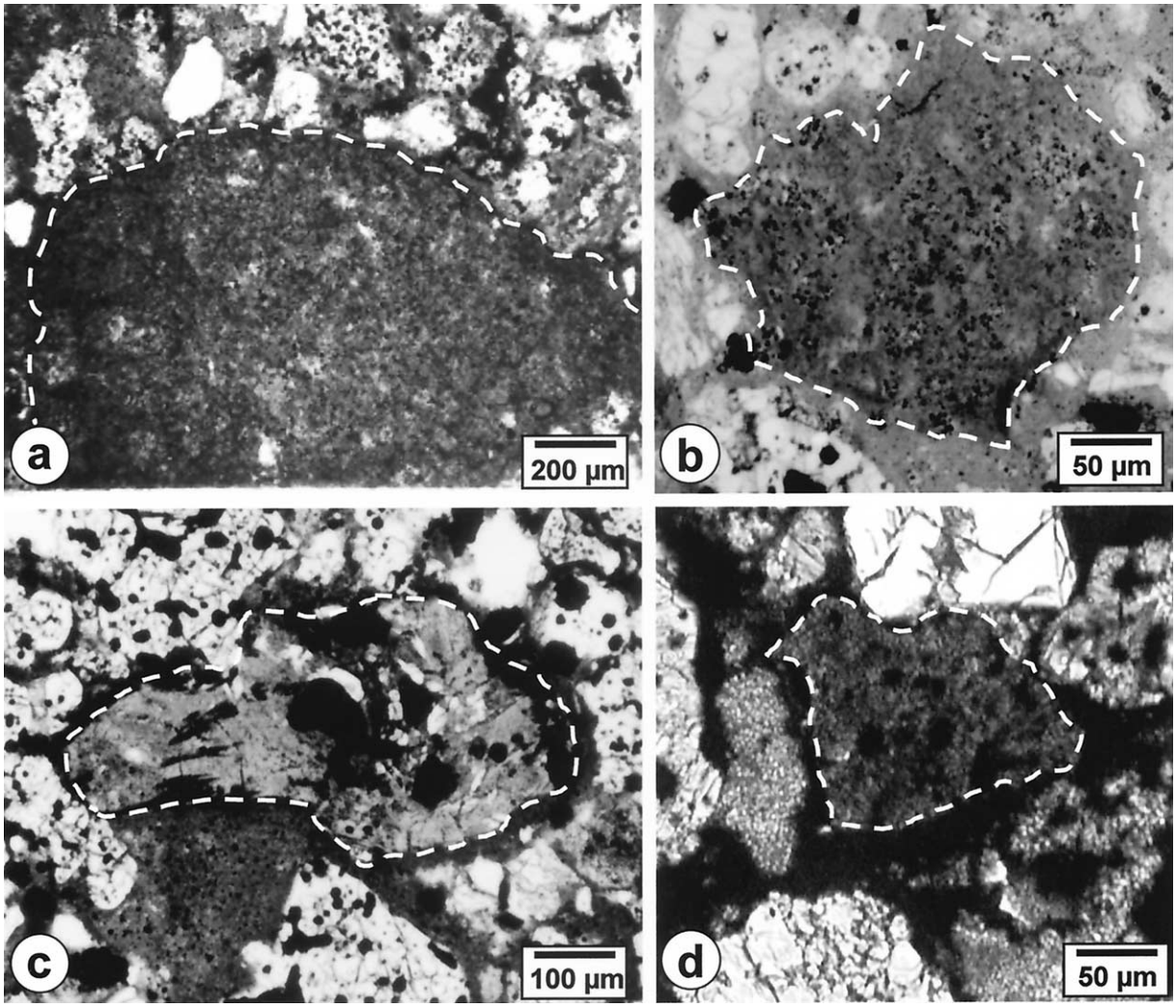

Fig. 1. Transmitted, plane-polarized light images of dark inclusions (DIs) (outlined by white broken lines) in the four CO3 chondrites. (a) Type II DI in Ornans, which is by far the largest (1200 × 500 μm) of all the DIs studied. (b) Type II DI in Warrenton. (c) Type I DI in Kainsaz. (d) Type I DI in Lancé.

in petrologic grade from 3.1 to 3.6 as a result of thermal metamorphism on their parent body (McSween, 1977a; Scott and Jones, 1990). Hence, if evidence of secondary processes was observed in the DIs, we also intended to determine the relationship between these processes and the parent-body thermal metamorphism.

2. TEXTURAL VARIATIONS OF DIs IN CV3 CHONDRITES (BRIEF SUMMARY OF PREVIOUS RESULTS)

To help readers understand the following descriptions, we here provide a brief summary of textural variations of DIs in CV3 chondrites. DIs in CV3 chondrites are commonly angular and range in size from a few millimeters to a few centimeters (Fruland et al., 1978; Johnson et al., 1990). They are lithic clasts that show a wide range of variation in texture. On the basis of texture, they can be mainly divided into four types; we call them types A, A/B, B, and C (Table 1), following the proposal of Krot et al. (1995). Type A and B constitute two end-members in a range of continuous variation in texture. Type A DIs contain chondrules, CAIs, and mineral fragments in a fine-grained matrix, so resembling the host CV3 chon-

Table 1. Classification of dark inclusions (DIs) in CV3 and CO3 chondrites.

CV3 type	Characteristics	CO3 type
A	Host chondrite-like material containing chondrules and Ca-Al-rich inclusions in a fine-grained matrix	
A/B	Intermediate between type A and B inclusions; chondrules are partially replaced by fine-grained aggregates	*
B	Consists entirely of fine-grained material containing chondrule-shaped aggregates in a matrix	I
C	Consists entirely of fine-grained material lacking chondrule-shaped aggregates	II

* Type I DIs containing coarse-grained objects (chondrule remnants).

Table 2. Dark inclusions (DIs) in the four CO3 chondrites.

Sample	Petrologic type	No. of DIs[a]		Diameter[b] (average) (μm)	Studied area (mm^2)	Modal abundance (vol. %)
		Type I	Type II			
Kainsaz	3.1	18	9	50 to 380 (130)	107	0.6
Ornans	3.3	2	32	50 to 850 (160)	109	1.2 (0.6)[c]
Lancé	3.4	4	21	75 to 290 (150)	178	0.7
Warrenton	3.6	1	14	80 to 340 (170)	67	0.7

[a] Inclusions smaller than 50 μm are not included.
[b] Average of two dimensions.
[c] The value in parenthesis is obtained by excluding the exceptionally large DI (850 μm) shown in Figures 1a and 9a.

drites. Type B DIs consist mostly of fine-grained, homogeneous, Fe-rich olivine and lack chondrules and CAIs; instead, they contain rounded, porous aggregates of fine-grained, Fe-rich olivine that are similar in size and shape to chondrules (Kojima and Tomeoka, 1996). Type A/B DIs have a texture that is intermediate between these two end-members; i.e., in this type of DI, chondrules are partly replaced by porous aggregates of fine-grained olivine. This type of DI is the most common and shows a wide range of variation in volume proportion of unreplaced coarse-grained materials and replaced fine-grained materials. Type C DIs consist mostly of fine-grained, Fe-rich olivine; coarse-grained components and chondrule-shaped porous aggregates are absent, so they are almost featureless in texture.

3. MATERIALS AND METHODS

The samples used for this study are four polished thin sections of the CO3 chondrite falls Kainsaz, Ornans, Lancé, and Warrenton. Thin sections of Kainsaz and Ornans were provided by the Smithsonian Institution (USNM 2486-7 and USNM 1105-2, respectively) and those of Lancé and Warrenton by the Natural History Museum, Vienna (L3413 and L6617, respectively). They were studied using an optical microscope, a SEM (JEOL JSM-5800) equipped with an energy-dispersive X-ray spectrometer (EDS), and an electron probe microanalyzer (JEOL JXA-8900) equipped with wavelength-dispersive X-ray spectrometers (WDSs). Data corrections were made by the phi-rho-Z method for EDS analysis and by the Bence-Albee method for WDS analysis. EDS analyses were obtained at 15 kV and 0.4 nA and WDS analyses at 15 kV and 12 nA. Well-characterized natural and synthetic minerals and glasses were used as standards. For the analysis of each mineral grain, we used a focused electron beam of ~2 μm in diameter. For the analysis of fine-grained DIs and matrices, we used a defocused electron beam of ~30 μm in diameter; this beam size is regarded to be optimum to obtain bulk compositions of DIs, considering their size and shape.

4. PETROGRAPHY AND MINERALOGY

4.1. General Petrography

Totals of 27, 34, 25, and 15 fine-grained inclusions have been found in each thin section of Kainsaz, Ornans, Lancé, and Warrenton, respectively (Table 2, Figs. 1a to 1d). They are brownish to grayish and translucent in transmitted light, and they have an appearance similar to the matrix of each host meteorite. The DIs are commonly rounded in shape; those having angular to irregular morphologies are relatively minor in abundance. They range in diameter from 50 to 850 μm, but ~87% of them are in the range between 50 and 200 μm; inclusions $<$ 50 μm in diameter were not included in our survey because of difficulty in precise identification. The size distributions of DIs in the four chondrites are generally similar to one another, with averages of 130 to 170 μm (Fig. 2). Modal abundances of DIs in the four chondrites range from 0.6 to 1.2 vol.% (Table 2); if an exceptionally large DI (~850 μm) in Ornans is excluded, the modal abundances are in the narrow range of 0.6 to 0.7. Although the general appearance of DIs resembles that of DIs in CV3 chondrites, they are significantly different in size. Most DIs previously reported from CV3 chondrites are a few millimeters to a few centimeters in size and easily recognized in hand specimens (e.g., Fruland et al., 1978; Johnson et al., 1990), whereas most DIs in the CO3 chondrites that we found are generally too small to recognize in hand specimens.

In back-scattered electron images, differences between DIs and surrounding matrices are more obvious. The DIs are porous aggregates composed mainly of fine grains ($<$1 to 20 μm in diameter) of Fe-rich olivine ($Fa_{35\ to\ 80}$) (Table 3). The olivine grains are clearly different in size and morphology from those in the matrices, as described later, and the boundaries between DIs and the host meteorites are sharp. Especially in Kainsaz, which is the least equilibrated among the four CO3 chondrites, DIs tend to be more enriched in Fe than the matrix and so appear distinctly brighter in back-scattered electron images than the surrounding matrix (Figs. 3 to 5). The DIs contain minor amounts of fine grains of Fe-Ni metal (kamacite and taenite, $<$1 to 80 μm in diameter), diopside, Fe-poor olivine ($Fa_{1\ to\ 25}$) (5 to 40 μm), troilite, magnetite, and nepheline ($<$1 to 20 μm) (roughly in the order of abundance) (Tables 3 and 4).

The DIs show a wide range of variation in texture and mineralogy, but they can be mostly classified into two types, which we hereafter call type I and type II. Type I DIs contain rounded to oval-shaped objects (typically 10 to 40 μm in diameter) of porous aggregates of fine grains ($<$1 to 3 μm) in a fine-grained matrix (Figs. 3a to 3c and 4a to 4c); some DIs consist entirely of assemblages of rounded objects with little interstitial matrix. On the other hand, type II DIs consist entirely of fine-grained, matrix-like material and are devoid of rounded objects. Type I DIs are generally less porous than type II DIs. There are also DIs that appear to be intermediate between the two types, e.g., a type II DI that is partly attached to a type I DI and a type I DI that is surrounded by a type II DI–like rim. Type I DIs are more abundant than type II DIs in Kainsaz, whereas type II DIs are predominant in Ornans, Lancé, and Warrenton (Table 2). No significant differences in texture and mineralogy are observed in each of type I DIs and

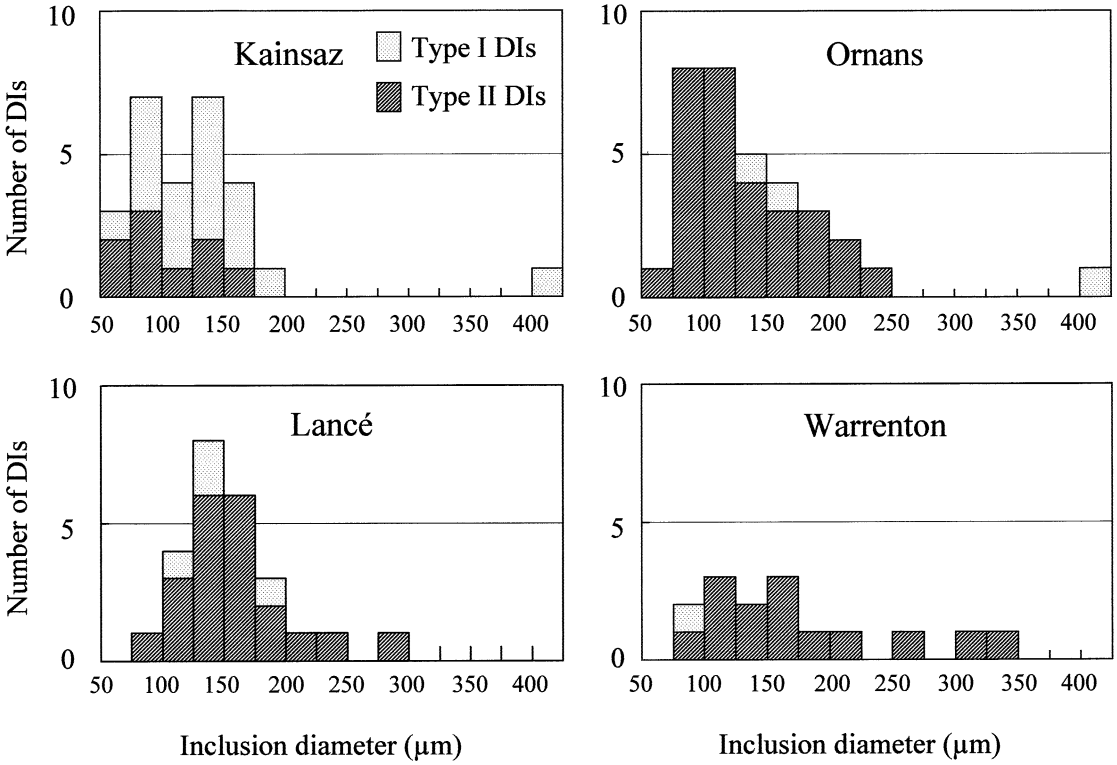

Fig. 2. Size distributions of dark inclusions (DIs) in the four CO3 chondrites. The size of each DI is an average of two dimensions. One (850 μm) in Ornans is out of the range. Inclusions smaller than 50 μm are not included in our survey.

type II DIs among the four meteorites. So, in the following, the texture and mineralogy of two types of DIs in all the four meteorites are described together, unless they are otherwise specified.

4.2. Type I DIs

Rounded to oval-shaped objects in this type of DI consist of fine anhedral to equidimensional grains of Fe-rich olivine (<1 to 3 μm in diameter) (Fig. 3c) and also commonly consist of parallel stacks of thin lath to needle-shaped grains (typically 1 to 3 μm in thickness, 10 to 15 μm in length, and 4 to 10 in aspect ratio) of Fe-rich olivine (Fig. 4b). Each rounded object is commonly outlined by a thin rim ($\sim$1 μm in thickness) of olivine (Fig. 3c) and is more clearly discernible in transmitted crossed polarized light (Figs. 4d and 4e). The fine olivine grains within each object exhibit simultaneous extinction, which indicates that they have a common crystallographic orientation. Rounded objects in some DIs in Kainsaz have coarse-grained cores (5 to 10 μm in diameter) of Fe-poor olivine ($Fa_{5\ to\ 25}$) (Fig. 3c, Table 3). Those Fe-poor olivine cores show Fe-Mg zoning, and the core and the surrounding fine-grained rim in each object are materially continuous. Some DIs contain optically opaque, rounded to oval-shaped nodules (10 to 30 μm in diameter) that are composed of intimate mixtures of Fe-Ni metal, troilite, magnetite, Fe-rich olivine, and occasionally Ca-phosphate (Figs. 5b and 5c). Olivine grains surrounding those opaque nodules are commonly enriched in Fe ($Fa_{55\ to\ 70}$); thus, the nodules exhibit bright halos in back-scattered electron images (Fig. 5b). Metal and troilite are less abundant than in chondrules in the host meteorites.

Another characteristic feature of type I DIs is the occurrence of narrow veins that range in width from 1 to 6 μm and in length from 10 to 50 μm (Figs. 5c and 5d). They are commonly connected to one another, forming a network. The veins are filled with Fe-rich olivine, which is typically more Fe rich than surrounding olivine; those olivine grains tend to be elongated along the veins. Some veins show symmetrical distributions of thin olivine walls ($\sim$1 μm in thickness) with hollow central zones, exhibiting an appearance similar to a longitudinal section of a pipe (Fig. 5d). Most veins occur in interstices between rounded objects, but some penetrate them. Some veins extend from opaque-nodule-like objects (Fig. 5c). The veins terminate at the boundaries between DIs, and the host meteorites and never extend outward (e.g., Fig. 5c).

4.3. Type I DIs Containing Coarse-Grained Objects

Four type I DIs (three in Kainsaz and one in Ornans; $\sim$16% of all the type I DIs studied) contain rounded to irregularly shaped objects (60 to 100 μm in diameter), not all of them as central cores, that are mainly composed of coarse grains (5 to 40 μm) of Fe-poor olivine ($Fa_{1\ to\ 10}$) and/or enstatite. Enstatite is extremely rare in DIs but is contained in all the coarse-grained objects in the four DIs. A core in a Kainsaz DI shown in Figures 6a and 6b consists largely of enstatite grains (5 to 20 μm) with rounded opaque inclusions (1 to 10 μm), bearing a close resemblance to a porphyritic pyroxene chondrule. The

Table 3. Selected electron microprobe analyses of olivine, diopside, nepheline, and kirschsteinite in dark inclusions in the four CO3 chondrites (wt. %).

	Type I							Type II			
	Ol					Di	Ne	Ol			Kir
	K	K	K	K[a]	K[b]	K	K	O	L	W	O
SiO_2	35.0	34.7	31.7	34.5	39.8	54.7	44.7	34.3	35.8	35.4	34.5
Al_2O_3	0.50	0.44	0.40	0.09	0.13	1.64	33.9	0.10	0.58	0.07	n.d.
K_2O	0.13	0.15	0.15	n.d.	n.d.	n.d.	0.09	n.d.	0.12	n.d.	n.d.
TiO_2	0.32	0.33	0.32	n.d.	n.d.	0.71	0.26	n.d.	0.37	0.10	n.d.
FeO	38.4	44.0	56.3	45.3	16.8	0.49	0.53	44.4	35.9	35.2	26.0
MgO	23.9	18.7	8.63	19.2	43.0	22.2	0.37	19.8	24.7	28.3	7.36
CaO	0.45	0.41	0.56	0.13	0.15	19.8	1.52	0.06	0.65	0.34	30.7
MnO	0.90	0.78	1.45	0.52	0.15	0.57	0.41	0.47	0.84	0.24	0.24
NiO	0.33	0.34	0.31	n.d.	n.d.	0.09	0.20	0.05	0.39	n.d.	0.40
Cr_2O_3	0.19	0.20	0.19	0.07	0.07	0.28	0.13	0.21	0.56	0.12	0.23
Na_2O	0.41	0.34	0.32	0.28	0.23	n.d.	18.1	0.21	0.46	0.34	0.05
Total	100.5	100.3	100.3	100.2	100.4	100.3	100.2	99.7	100.6	100.2	99.6
Atomic ratios calculated as O = 24											
Si	5.92	6.02	5.93	6.05	6.03	7.74	6.28	5.96	5.99	5.93	6.09
Al	0.10	0.09	0.09	0.02	0.03	0.27	5.65	0.02	0.11	0.01	n.d.
K	0.03	0.03	0.04	n.d.	n.d.	n.d.	0.02	n.d.	0.03	n.d.	n.d.
Ti	0.04	0.04	0.05	n.d.	n.d.	0.08	0.03	n.d.	0.05	0.01	n.d.
Fe	5.44	6.39	8.82	6.76	2.13	0.06	0.06	6.66	5.02	4.93	3.84
Mg	6.04	4.83	2.41	5.07	9.71	4.67	0.08	5.30	6.15	7.07	1.94
Ca	0.08	0.08	0.11	0.03	0.02	2.99	0.22	0.01	0.12	0.06	5.83
Mn	0.15	0.13	0.23	0.08	0.02	0.07	0.05	0.07	0.12	0.03	0.04
Ni	0.04	0.05	0.05	n.d.	n.d.	0.01	0.02	0.01	0.05	n.d.	0.06
Cr	0.03	0.03	0.03	0.01	0.01	0.02	0.01	0.03	0.08	0.02	0.03
Na	0.14	0.11	0.12	0.07	0.05	n.d.	4.81	0.08	0.14	0.10	0.02

Ol = olivine, Di = diopside, Ne = nepheline, Kir = kirschsteinite, K = Kainsaz, O = Ornans, L = Lancé, W = Warrenton, n.d. = not determined.
[a] An olivine grain in a vein.
[b] A coarse-grained olivine core in a rounded object shown in Figure 3c.

boundary between the core and the surrounding fine-grained rim of Fe-rich olivine is very irregular; in places, the rim intrudes deeply into the core. Fe-Ni metal grains in both the interior and the edge of the core are partially replaced by very Fe-rich olivine ($Fa_{65\ to\ 75}$) (Fig. 6b). Figures 7a to 7c show a Kainsaz inclusion in which a coarse-grained object (in this case not a core) is partially replaced by fine-grained aggregates of Fe-rich olivine that are regarded as a type I DI. The coarse-grained object contains rounded grains of Fe-poor olivine that are poikilitically enclosed by enstatite, having a typical texture of porphyritic olivine-pyroxene chondrules (Fig. 7a).

A DI in Ornans shown in Figures 8a to 8g is texturally unique and, we believe, provides important information regarding the origin of type I DIs, so we describe it in detail. This DI has a core (~90 μm in diameter) consisting of coarse-grained single crystals of Fe-poor olivine (Fa_5) and a minor amount of enstatite enclosed by a two-layered, fine-grained rim. Each olivine grain in the core exhibits pronounced Fe-Mg zoning. The inner rim consists of very long, needle-shaped grains of Fe-rich olivine (12 to 15 in aspect ratio), and the outer rim consists of much smaller and more equidimensional grains of Fe-rich olivine. Our observations in transmitted light reveal that the area including the core and the inner rim consists of five distinct regions (A, B, C, D, and E in Figs. 8b and 8c). Within each region, most olivine needles are oriented in parallel to each other and are materially continuous to the outer edges of the coarse olivine grains in the core. A striking feature is that in transmitted crossed polarized light, both needles and coarse grains of olivine in each region exhibit simultaneous extinction (Figs. 8e and 8f), which indicates that they have a common crystallographic orientation. Olivine needles commonly contain numerous microinclusions (<0.2 μm in diameter) rich in Fe, Ni, and S, probably Fe-Ni metal and troilite, and microcavities (<0.2 μm), and are enclosed by minute grains of diopside and nepheline (Fig. 8g).

4.4. Type II DIs

This type of DI is almost featureless in transmitted plane-polarized light and is more similar in appearance to the matrices of the host CO3 chondrites than type I DIs (Figs. 1a and 1b). However, olivine grains in type II DIs differ distinctly in morphology and size from those in the matrices. Olivine grains in the DIs are commonly elongated, with aspect ratios of 3 to 12, and have sizes typically 1 to 2 μm in width and 6 to 12 μm in length (Figs. 9a to 9c), whereas olivine grains in the matrices of the host meteorites are more equidimensional in morphology and much smaller in size (mostly <1 μm). Olivine grains in type II DIs in Ornans generally have larger sizes and higher aspect ratios than those in other three chondrites. The elongated grains of olivine are nearly randomly oriented throughout inclusions. Veinlike features are absent in any type II DIs that we studied. Minor amounts of grains of Fe-poor olivine ($Fa_{5\ to\ 25}$) (5 to 40 μm in diameter), diopside (5 to 20 μm), Fe-Ni metal, and troilite (<1 to 5 μm) are dispersed in the DIs, although

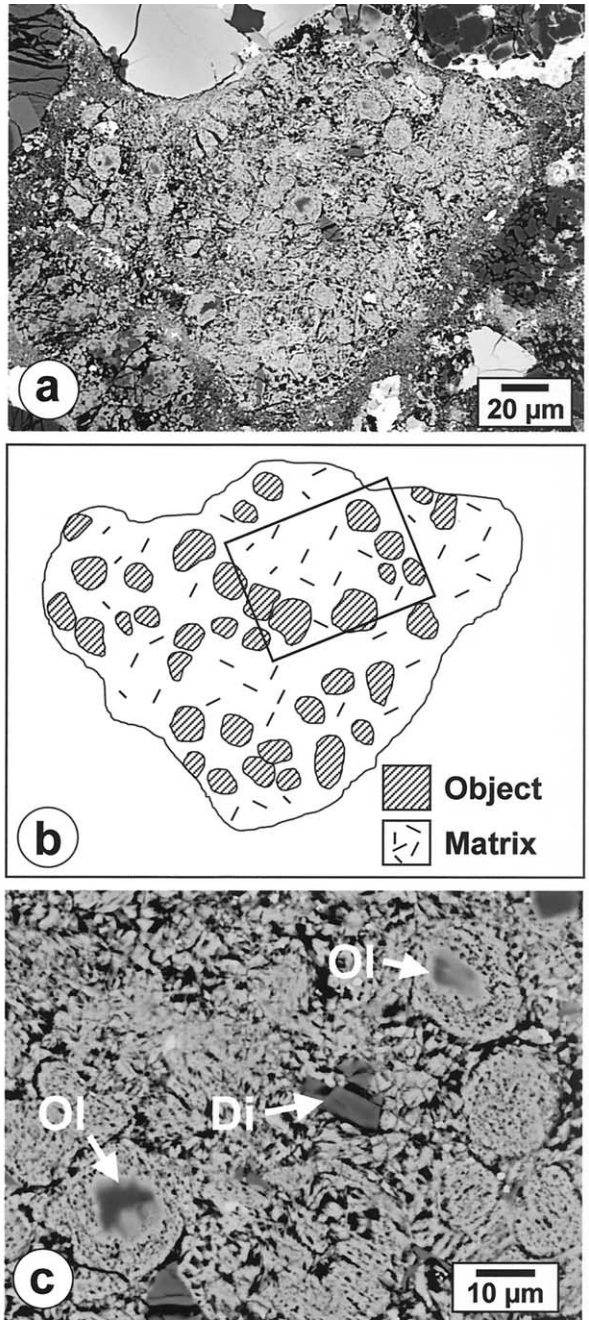

Fig. 3. (a) Back-scattered electron image of a type I dark inclusion (DI) in Kainsaz. (b) Illustration of the DI in (a) showing rounded objects in a matrix. (c) Image of boxed area in (b) showing rounded objects, each consisting of a porous aggregate of fine grains of Fe-rich olivine, embedded in a fine-grained matrix. Some rounded objects have coarse-grained cores of Fe-poor olivine (Ol) that exhibit Fe-Mg zoning. Note that a core and a surrounding fine-grained aggregate in each object are materially continuous. Also note that each object is outlined by a thin rim. Grains of diopside (Di) are dispersed in the DI matrix.

these accessory phases are much less common than in type I DIs.

A type II DI in Ornans (Figs. 1a and 9a to 9d) is 1200 × 500 μm in size, which is by far the largest of all the DIs studied. This DI consists entirely of fine, needle-shaped grains of Fe-rich olivine with very high aspect ratios (8 to 12) (Figs. 9b and 9c). It is enclosed by a 30- to 50-μm-thick rim that is composed of Fe-rich olivine grains having distinctly smaller grain sizes ($<$1 to 5 μm) and more equidimensional morphology than those in the interior DI (Fig. 9d). Olivine needles in the DI contain numerous microinclusions ($<$0.2 μm in diameter) rich in Fe, Ni, and S, and microcavities ($<$0.2 μm), and are enclosed by minute grains of diopside and nepheline (Fig. 9c). Focused-beam analyses of the olivine grains indicate that Fe and Ni are correlated, and so are Fe and S in distribution; thus, the microinclusions are probably Fe-Ni metal and troilite. These morphologic and textural characteristics of the olivine grains are almost identical to those in the type I DI in Ornans described above (cf. Fig. 8g). We also note that olivine grains in Allende DIs commonly contain numerous microinclusions of opaque phases and microcavities (cf. Fig. 12 in Kojima and Tomeoka, 1996; see also Brearley and Prinz, 1996 and Krot et al., 1997), similar to the olivine grains in the CO3 DIs. Irregularly shaped aggregates (10 to 50 μm in size) of kirschsteinite (Fig. 9b, Table 3) and Ca phosphate are contained in this DI and some other DIs in Ornans.

4.5. Chemical Compositions of DIs

Bulk major element compositions of DIs and the matrices in the four CO3 chondrites obtained by WDS defocused-beam analyses are shown in Table 5. We found no significant differences in composition between type I DIs and type II DIs in each of the four CO3 chondrites; e.g., the major element abundances of type I DIs and type II DIs in Kainsaz are compared in Figure 10. We treat the compositions of type I DIs and type II DIs in each chondrite together. Major element abundances of DIs in the four CO3 chondrites are compared to one another in Figure 11a and also to those of the Allende-AF DI (a type B DI in Allende; see Kojima and Tomeoka, 1996, for details) and chondrule-like inclusions in Allende-AF in Figure 11b. Although bulk compositions of DIs differ considerably in MgO and FeO contents between the four CO3 chondrites, elemental abundance patterns of DIs in the four chondrites are surprisingly similar to one another (Fig. 11a). The differences in MgO and FeO can be largely ascribed to thermal metamorphism of the host meteorites, as described below. The elemental abundance patterns, however, differ distinctly from that of bulk CO3 chondrites (Fig. 11a). Compared to bulk CO3 chondrites, DIs are enriched in Mn and Ti approximately by factors of 4 and 3 and depleted in Ca, S, and Ni by factors of 2, 2, and 3, respectively. The elemental abundance patterns of DIs show a general resemblance to that of Allende-AF and more closely to that of chondrule-like inclusions in Allende-AF (Fig. 11b).

To estimate the effects of thermal metamorphism of the host meteorites on DIs, we performed defocused-beam analysis of DIs and the host meteorite matrices at a constant area density (one analysis/100 × 100 μm) using a 30-μm diameter beam (Fig. 12). Although olivine compositions are the most useful diagnostic property to determine the effects of thermal metamorphism (Scott and Jones, 1990), it is not possible to perform a focused-beam analysis of individual olivine grains in DIs because of their small grain size. It is obvious, however, that the distributions of FeO/(FeO + MgO) ratios determined by the defocused beam analyses are largely related to the composi-

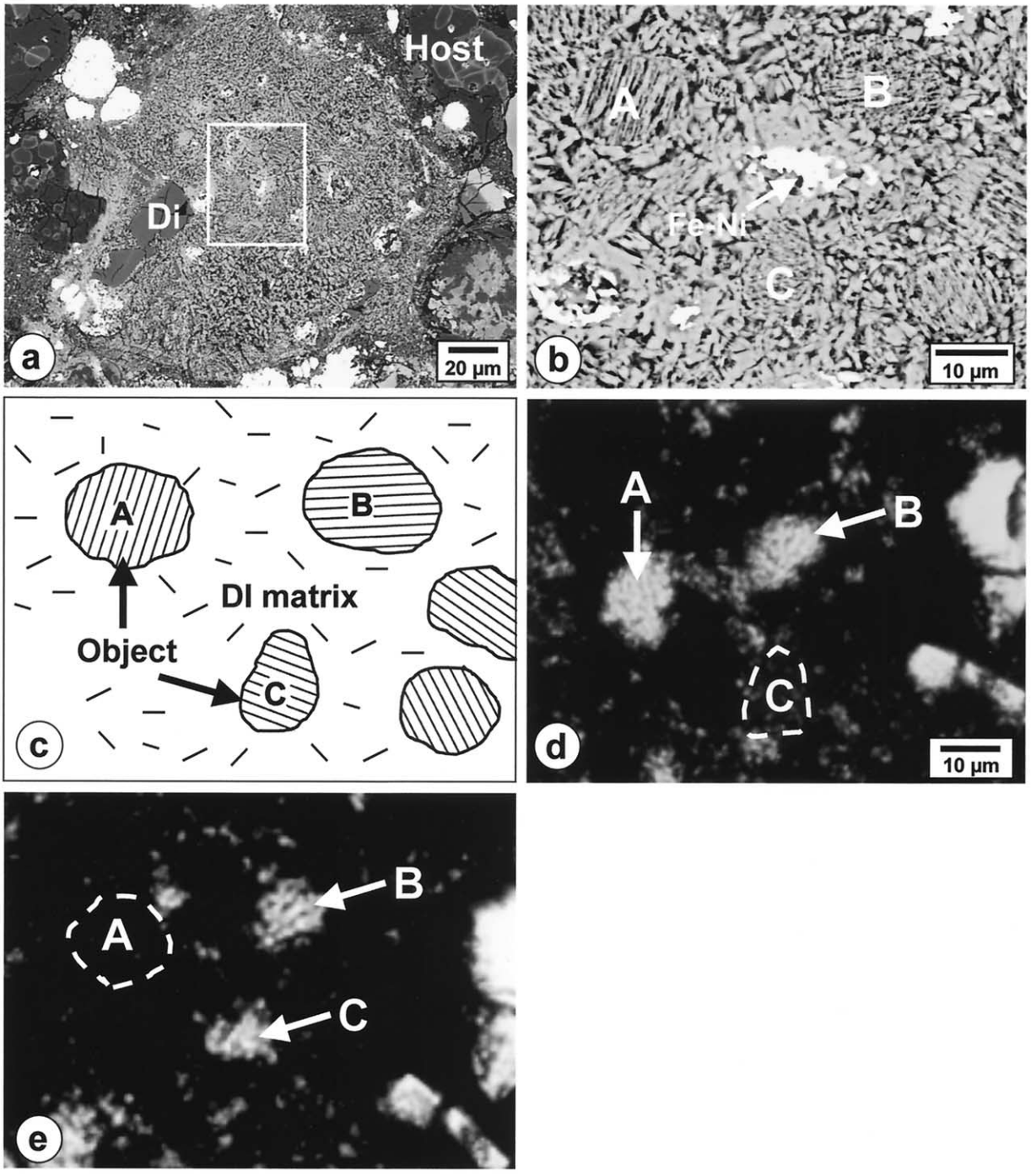

Fig. 4. (a) Back-scattered electron image of a type I dark inclusion (DI) in Kainsaz. (b) Image of boxed area in (a) showing rounded objects, each consisting of parallel stacks of needle-shaped grains, embedded in a fine-grained matrix. (c) Illustration of the image in (b). Labeled objects correspond to those in (b). (d) The same area as in (b) in transmitted crossed polarized light. (e) Forty-five-degree-rotated image of the same area. Note that all fine grains of olivine in object A become extinct simultaneously, while those in object C become transparent. Di = diopside. Fe-Ni = Fe-Ni metal.

tions of olivine, the predominant phase, in DIs and the matrices and so reflect the effects of thermal metamorphism. Our analyses of the matrices in Kainsaz, Ornans, and Warrenton are generally similar to the analyses of individual matrix olivines in those meteorites obtained using a transmission electron microscope (Brearley and Jones, 1998). Our analyses show that there are significant differences among the four meteorites. DIs in Kainsaz are heterogeneous, with no apparent peak in distribution of FeO/(FeO + MgO) weight ratios, ranging from 58 to 87%. The matrix in Kainsaz is similarly heterogeneous, although it tends to be poorer in Fe than DIs. On the other hand, both DIs and the matrices in Ornans, Lancé, and Warrenton are

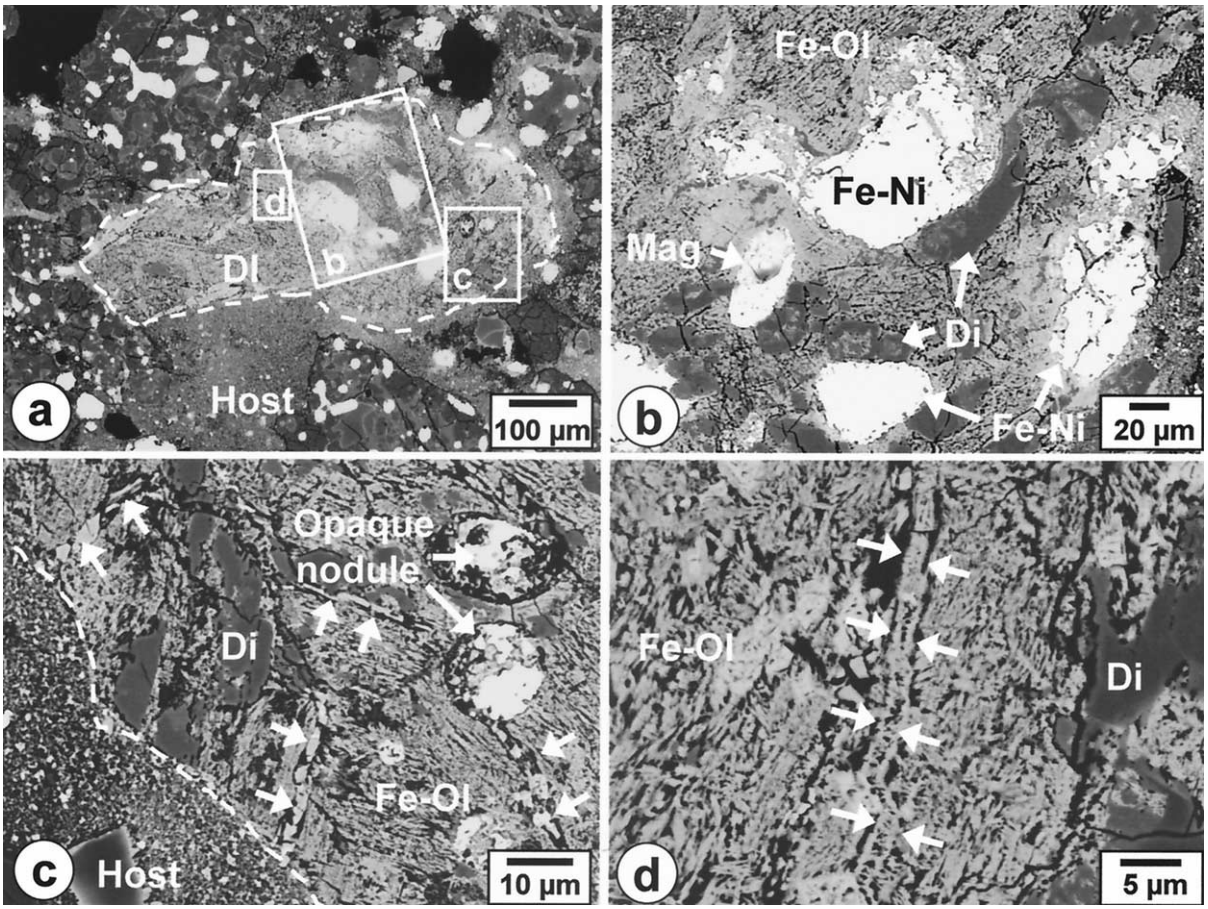

Fig. 5. (a) Back-scattered electron image of a type I dark inclusion (DI) in Kainsaz shown in Figure 1c. (b) Image of boxed area b in (a) showing abundant grains of Fe-Ni metal (Fe-Ni) and magnetite (Mag). Note that those opaque mineral grains exhibit bright Fe-rich halos. (c) Image of boxed area c in (a) showing a network of veins of Fe-rich olivine (Fe-Ol) (marked by arrows). Some veins extend from opaque nodules. Veins terminate at the boundary between the DI and the host meteorite (white broken line). Also note that fine elongated grains of Fe-rich olivine (gray) are oriented roughly parallel to one another. (d) Image of boxed area d in (a) showing that a vein (marked by arrows) has a symmetrical distribution of thin olivine walls with a hollow central zone. Di = diopside.

much more homogeneous than those in Kainsaz. There are no significant differences between DIs and the matrix in each of these three meteorites, and the FeO/(FeO + MgO) ratio tends to decrease as the petrologic type of the host meteorite increases.

4.6. Opaque Mineralogy in DIs

Opaque minerals, mostly Fe-Ni metal (kamacite and taenite), troilite, and magnetite, occur as accessory minerals in DIs. Although minor in abundance, opaque minerals differ distinctly

Table 4. Average compositions of metals in the four host CO3 chondrites and dark inclusions (DIs) in those chondrites (microprobe analyses, wt. %).

		Kamacite				Taenite			
		No. of grains (no. of DIs)	Ni	Co	Cr	No. of grains (no. of DIs)	Ni	Co	Cr
Kainsaz	host		4.5	0.6	0.36		46.4		
	DIs	21 (8)	4.3	0.6	0.33	13 (5)	47.3	0.2	0.18
Ornans	host		—	—	—		60.9		
	DIs	0 (0)	—	—	—	16 (9)	61.3	1.2	0.08
Lancé	host		5.3	1.0	0.10		41.2		
	DIs	23 (10)	4.6	0.8	0.11	18 (7)	42.3	0.3	0.11
Warrenton	host		6.3	1.5	0.0		39.6		
	DIs	22 (10)	6.1	1.4	0.06	16 (6)	41.1	0.6	0.06

Data of host chondrites from McSween (1977a).

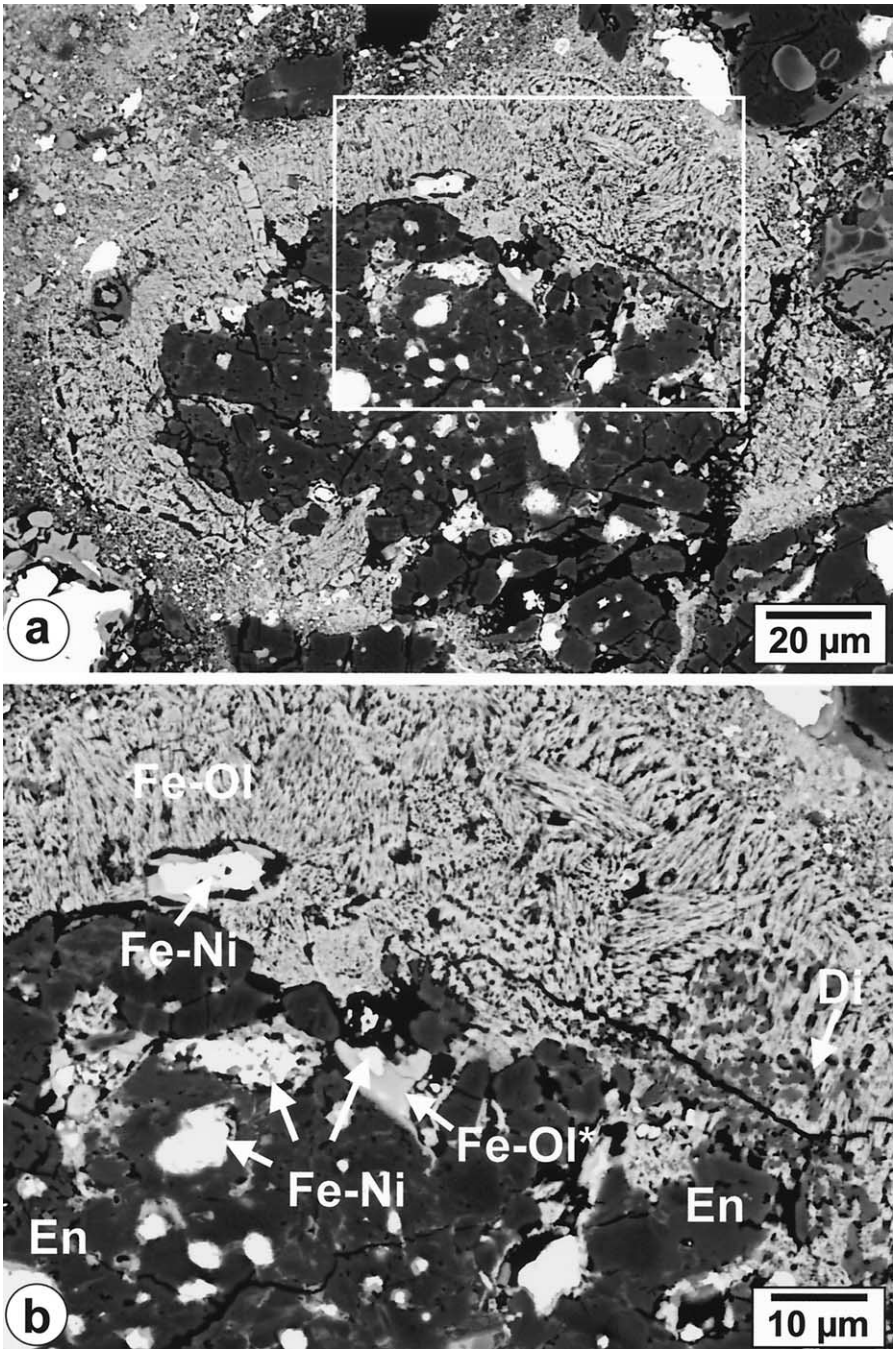

Fig. 6. (a) Back-scattered electron image of a type I dark inclusion (DI) containing a coarse-grained core in Kainsaz. The core consists largely of enstatite grains with rounded inclusions of Fe-Ni metal (Fe-Ni) (bright), having a texture similar to a porphyritic pyroxene chondrule. (b) Image of the boxed area in (a) showing an irregular boundary between the core and the surrounding fine-grained rim of Fe-rich olivine (Fe-Ol). Fe-Ni metal grains near the edge of the core are partially replaced by very Fe-rich olivine ($Fa_{65\ to\ 75}$, Fe-Ol*). En = enstatite, Di = diopside.

between meteorite types and so potentially serve as good indicators for understanding the relationship between DIs and the host and other types of meteorites. Among the opaque phases, Fe-Ni metal in particular shows considerable variations in mineralogy and composition among DIs in the four chondrites. DIs in Kainsaz, Lancé, and Warrenton contain kamacite and taenite, whereas DIs in Ornans contain no kamacite, only high-Ni taenite. Those metallic phases were analyzed for Fe, Ni, Co, and Cr (Table 4). Kamacite grains in DIs in the three chondrites contain 4.3 to 6.1 wt.% Ni, 0.6 to 1.4 wt.% Co, and 0.06 to 0.33 wt.% Cr in average content. Taenite grains in DIs in the same three chondrites contain 41.1 to 47.3 wt.% Ni, whereas taenite grains in DIs in Ornans contain 61.3 wt.% Ni. The occurrence of minerals and the compositional characteristics of Fe-Ni metal in DIs in each

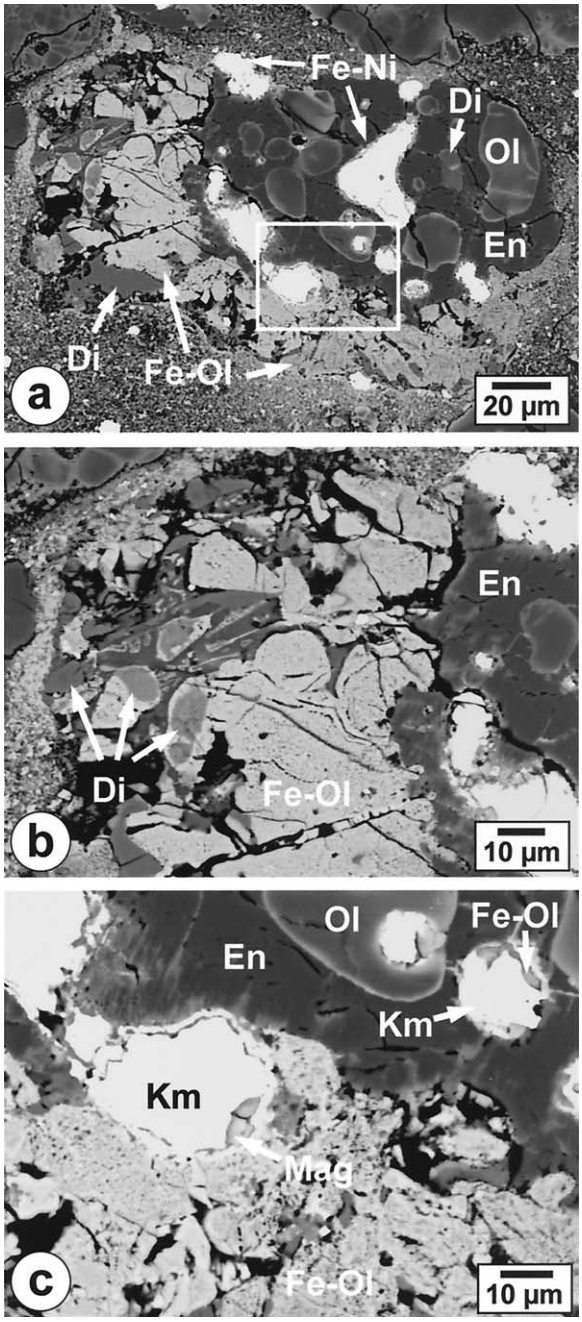

Figure 7. (a) Back-scattered electron image of an inclusion in Kainsaz consisting of a chondrule-like object and fine-grained, porous aggregates of Fe-rich olivine (Fe-Ol) (bright grayish portion) that are regarded as a type I dark inclusion (DI). In the chondrule-like aggregate, rounded olivine (Ol) grains are poikilitically enclosed by enstatite (En). (b) Image of the upper-left portion of (a) showing irregular contact between enstatite and fine-grained aggregates of Fe-rich olivine. The texture suggests that the enstatite is partially replaced by the aggregates of Fe-rich olivine. Diopside (Di) grains remain unaltered within the aggregates of Fe-rich olivine, suggesting that diopside is more resistant to alteration than enstatite. (c) Image of boxed area in (a) showing a kamacite (Km)–bearing nodule in direct contact with fine-grained aggregates of Fe-rich olivine. The kamacite is only partially replaced by magnetite (Mag). The texture suggests that kamacite resists alteration at least as well as enstatite does. Fe-Ni = Fe-Ni metal.

of the four CO3 chondrites are almost identical to those in their own host CO3 chondrites (Table 4).

5. DISCUSSION

5.1. Formation of Type I DIs

Type I DIs were found to contain peculiar rounded objects that consist largely of fine-grained, Fe-rich olivine that is commonly elongated in the same direction. These textural characteristics resemble those of chondrule-like inclusions in type B DIs in CV3 chondrites, although the size of the DIs is smaller in the CO3 chondrites (e.g., compare Figs. 3a to 3c and 4a to 4c to Figs. 6a and 6b in Kojima et al., 1993, and Figs. 3a to 3c in Kojima and Tomeoka, 1996). Kurat et al. (1989) suggested that those inclusions are aggregates of direct condensates from a gas in the solar nebula and that chondrules were formed from those inclusions. In contrast, Kojima and Tomeoka (1996) suggested that they are pseudomorphs of chondrules that formed during aqueous alteration and subsequent dehydration on the parent body. Our study provides abundant evidence suggesting parent-body processes that are similar to those for DIs in CV3 chondrites. We especially note the striking fact that all fine grains of olivine in each rounded object in the DIs have a common crystallographic orientation. It is extremely difficult to imagine that olivine particles in the solar nebula would stick to one another in such a way that their crystallographic orientations would be so uniform. Rather, this fact suggests that the rounded objects are pseudomorphs of phenocrysts in chondrules.

The coarse-grained-core-bearing DI shown in Figures 8a to 8g in particular provides evidence that such replacement reactions occurred and gives insights into how the uniformly oriented, fine olivine grains were formed from a single coarse crystal of olivine. In each of the regions A, B, C, D, and E in the DI, both coarse grains (unaltered relicts) and fine needle-shaped grains (alteration products) of olivine are materially continuous and have a common crystallographic orientation. This extraordinary texture suggests that both coarse and fine needle-shaped grains in each region were originally part of the same single crystal (i.e., a phenocryst) and that the single crystal was topotactically transformed, from its outer margin, to fine-grained, needle-shaped crystals. The needle-shaped grains of olivine appear to be elongated along a certain crystallographic direction of olivine, although the direction is unknown. This textural evidence suggests that the rounded objects consisting of uniformly oriented fine olivine grains in other type I DIs (Figs. 3 to 5) also resulted from a similar replacement process. The coarse-grained cores of Fe-poor olivine in the rounded objects shown in Figure 3c are probably unaltered relicts of olivine phenocrysts in chondrules, and the opaque phase–rich rounded objects, in which metals are partially replaced by Fe-rich olivine and magnetite (Fig. 5c), are relicts of opaque nodules in chondrules. There is also textural evidence that enstatite in the coarse-grained objects that are part of type I DIs is partially replaced by aggregates of fine-grained Fe-rich olivine (Figs. 6 and 7). However, information regarding enstatite is still too limited to allow us to infer how the uniformly oriented, fine olivine grains were formed from it.

From these observations, we suggest that the coarse-grained objects in the type I DIs shown in Figures 6 to 8 are unaltered

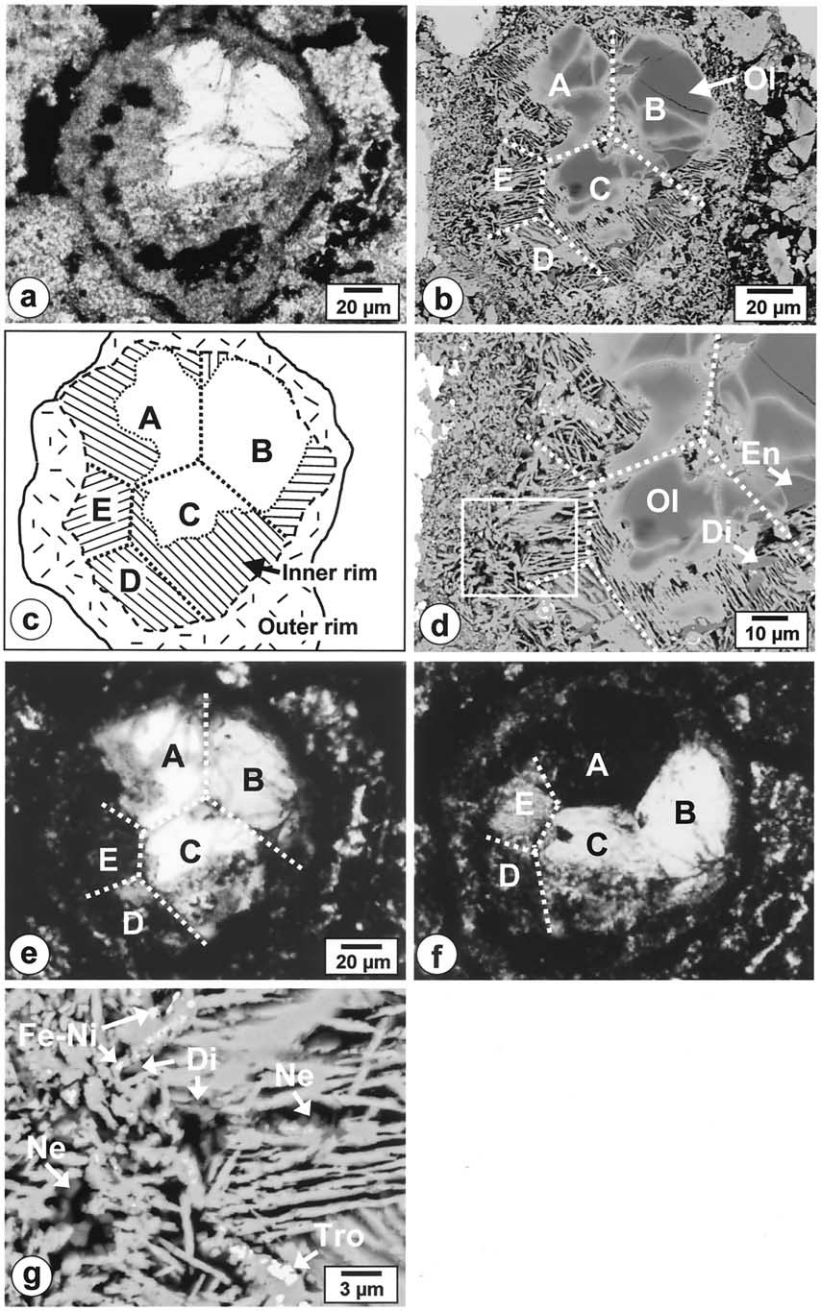

Fig. 8. (a) Transmitted, plane-polarized light image of a type I dark inclusion (DI) containing a coarse-grained core (transparent area) in Ornans. (b) Back-scattered electron image of the same DI as in (a), showing that the DI consists of a core enclosed by a two-layered, fine-grained rim. The core consists mainly of Fe-poor olivine (Ol) grains that have strong Fe-Mg zoning. The area including the core and the inner rim consists of five distinct regions: A, B, C, D and E. In each region, most olivine needles in the inner rim are oriented in parallel to one another. (c) Illustration of the DI in (b). The directions of parallel lines in the inner rim correspond to the directions of olivine needles. (d) Enlarged image of a lower left portion of (b) showing that the coarse grains (in the core) and needles (in the inner rim) of olivine show irregular contacts, suggesting that the former are replaced by the latter. (e) The same area as in (a) and (b) in transmitted, crossed polarized light. (f) Forty-five-degree-rotated image of the same area in (e) showing that both coarse grains and needles of olivine in region C become extinct simultaneously. The same phenomenon was observed in all the other regions at different rotation angles. (g) High-magnification image of the boxed area in (d) showing that olivine needles contain microinclusions of Fe-Ni metal (Fe-Ni) and troilite (Tro) (bright, some are marked by arrows) and microcavities (dark), and are enclosed by minute grains of diopside (Di) and nepheline (Ne) (dark grayish). En = enstatite.

remnants of chondrules. Thus, those coarse-grained-object-bearing DIs correspond to type A/B DIs (intermediate between type A and type B) in CV3 chondrites (see Table 1).

Another important characteristic that suggests parent-body processes is the presence of networks of veins filled with Fe-rich olivine. Veins consisting of Fe-rich olivine and Ca-Fe-

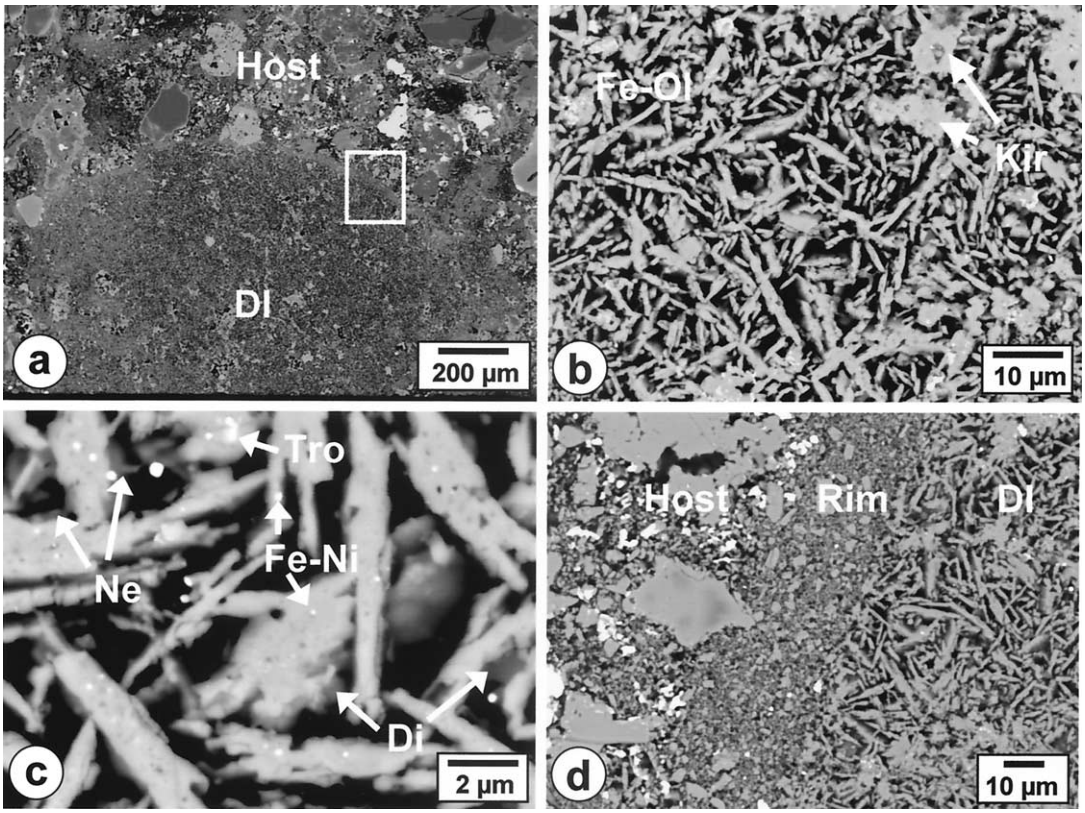

Fig. 9. (a) Back-scattered electron image of a type II dark inclusion (DI) in Ornans shown in Figure 1a. (b) Image of a portion of the DI showing that highly elongated grains of olivine are randomly oriented. Irregularly shaped grains of kirschsteinite (Kir) occur in places. (c) High-magnification image showing that olivine grains contain numerous microinclusions of Fe-Ni metal and troilite (bright) and cavities (dark) and are enclosed by minute grains of diopside (Di) and nepheline (Ne) (dark grayish). Note that the texture of individual olivine grains resembles that of olivine grains in the type I DI shown in Figure 8g. (d) Image of the boxed area in (a) showing that the DI is enclosed by a rim that is composed of fine olivine grains that are much smaller in size and more equidimensional in morphology than those in the interior of the DI.

rich pyroxene have been reported to be common in DIs in Allende (Kojima and Tomeoka, 1996; Krot et al., 1998). Many of the veins in DIs in the CO3 chondrites and Allende have a characteristic texture in common, including the longitudinal section of a pipelike texture (Fig. 5d; cf. Fig. 13b in Kojima and Tomeoka, 1996, and Figs. 11a and 11c in Krot et al., 1998). Those veins were probably formed by precipitation of minerals from a fluid onto the walls of fractures and so provide strong evidence that the DIs have experienced fluid-assisted alteration on the parent body. The fluid could have been either liquid or vapor. Based on the analogy with CI chondrites (Richardson, 1978; Tomeoka, 1990), we suggest that the veins formed in the presence of aqueous solutions. However, the DIs lack typical products of aqueous alteration, such as hydrous phyllosilicates. This lack can be explained by supposing that the DIs have gone through a dehydration process after aqueous alteration, just as in the case of DIs in CV3 chondrites. The veins terminate at the boundaries between DIs and the host meteorites, which indicates that aqueous alteration occurred before incorporation of DIs to the present location.

Fe-rich olivine grains in both type I and type II DIs commonly contain numerous microinclusions of opaque phases and microcavities (Figs. 8g and 9c). This is another unusual characteristic shared with many DIs in CV3 chondrites and provides additional evidence arguing against a nebular condensation origin for the DIs. As suggested by previous authors (Kojima and Tomeoka, 1996; Krot et al., 1999), we infer that those microinclusions and microcavities were formed during aqueous alteration and subsequent dehydration.

The DIs contain Fe-Ni metal grains, both kamacite and taenite. Because metal is regarded as being relatively susceptible to alteration, we consider what its presence implies. In type I DIs, metal mostly occurs as opaque nodules in which kamacite is commonly corroded and partially replaced by Fe-rich olivine, magnetite, and taenite (Figs. 5a to 5c). Metal-rich opaque nodules are also contained in the coarse-grained, chondrule-like objects in type I DIs, in which kamacite is less corroded (Figs. 6 and 7). In Allende, Fe-Ni metal occurs in type A DIs (weakly altered type), whereas it is rare in type B DIs (heavily altered type) (Fruland et al., 1978; Johnson et al., 1990; Kojima and Tomeoka, 1996; Krot et al., 1997, 1998). In Vigarano and Efremovka, however, Fe-Ni metal occurs even in type B DIs (Kojima et al., 1993; Krot et al., 1999). In Vigarano, Fe-Ni metal also occurs in a type C DI (Tomeoka and Kojima, 1998). Vigarano and Efremovka are among the members of the reduced subgroup of CV3 type, whereas Allende is a member

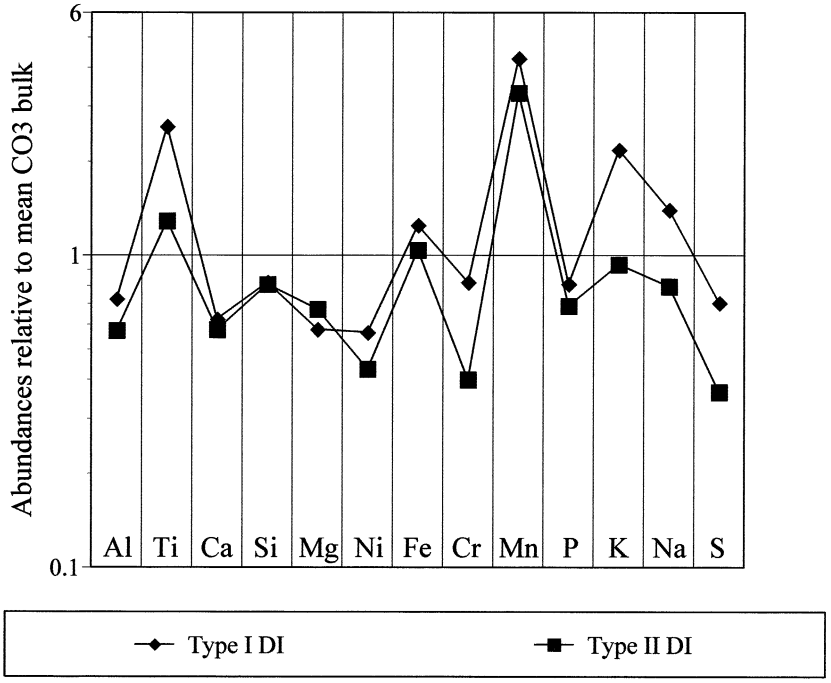

Fig. 10. Bulk chemical compositions of type I dark inclusions (DIs) and type II DIs in the Kainsaz CO3 chondrite obtained by wavelength-dispersive X-ray spectrometry defocused-beam analyses. Data are normalized to mean bulk CO3 values (from Rubin et al., 1985).

of the oxidized subgroup (McSween, 1977b). From these observations, we infer that the DIs in the CO3 chondrites were probably altered in relatively reducing conditions and that the metal-rich nodule-bearing type I DIs represent incompletely pseudomorphed chondrules. In the DI shown in Figure 7c, kamacite that is in contact with the replaced portion of enstatite is only partially replaced by magnetite, which suggests that kamacite resists alteration at least as well as enstatite does.

Our compositional analyses indicate that the bulk major element compositions of DIs are similar to that of the Allende-AF DI and even more similar to that of chondrule-like inclusions in Allende-AF (Fig. 11b). This result also suggests that type I DIs in the CO3 chondrites are related in origin to the Allende-AF DI.

5.2. Formation of Type II DIs

Type II DIs consist entirely of fine grains of Fe-rich olivine that are commonly elongated and contain neither chondrules nor chondrule pseudomorphs. The fine elongated grains are randomly oriented throughout inclusions. These textural characteristics resemble those of the fine-grained, matrix-like DIs in CV3 chondrites that are classified as type C DIs (Table 1) (Johnson et al., 1990; Krot et al., 1995). We also note that the randomly oriented texture of elongated olivine grains rather resemble those of the matrices of Vigarano DIs (Fig. 4 in Kojima et al., 1993) and some CV3 chondrites (Fig. 9 in Krot et al., 1998). From the texture, it is obvious that the origin of this type of DI cannot be explained by direct replacement of a chondritic precursor, and their formation process is less clear than that of type I DIs. Tomeoka and Kojima (1998) studied a type C DI in Vigarano (AMNH 2226-7) and showed that fine grains of olivine in AMNH 2226-7 bear a close resemblance in morphology, grain size, and chemical composition to those in type B DIs in Vigarano (Kojima et al., 1993) but are clearly different from those in the host meteorite matrix. So, they suggested that the fine olivine grains in AMNH 2226-7 resulted from size sorting and subsequent reassembly of grains that had been produced by disaggregation of a type B DI–like material.

We believe that it is significant that the bulk chemical compositions of type I DIs and type II DIs in each CO3 chondrite are closely similar to each other (Fig. 10). In addition, olivine grains in both types of DIs have many unusual characteristics in common: They commonly exhibit highly elongated morphology, with aspect ratios of 8 to 12; contain numerous microinclusions of Fe-Ni metal and troilite and microcavities; and are enclosed by minute grains of diopside and nepheline (Figs. 8g and 9c). All these characteristics suggest that there is a close genetic relationship between type I DIs and type II DIs. An important question is how the relationship of different textures of fine olivine needles in type I DIs (parallel oriented within rounded objects) and type II DIs (randomly oriented) can be explained. We envisage that type II DIs in the CO3 chondrites were formed by reassembly of fine grains that had resulted from disaggregation of a type I DI rock. Although we are uncertain as to how those processes took place, it is plausible that they are a kind of sedimentation process that occurred by the activity of aqueous solutions or gases internally in the CO parent body, as suggested by Tomeoka and Kojima (1998) for the type C DI in Vigarano.

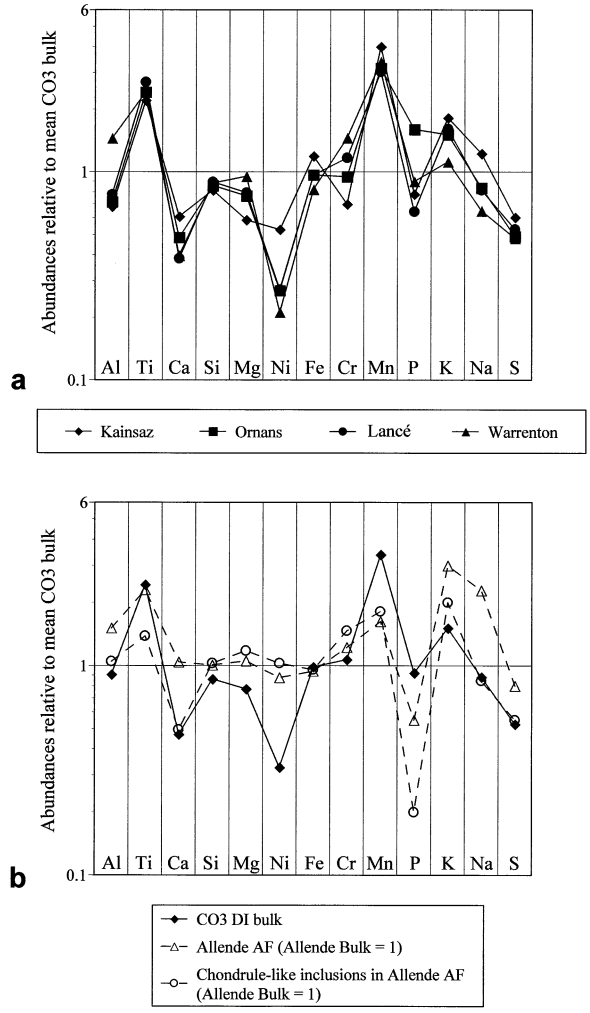

Fig. 11. (a) Bulk chemical compositions of dark inclusions (DIs) in the four CO3 chondrites obtained by wavelength-dispersive X-ray spectrometry defocused-beam analyses. Data are normalized to mean bulk CO3 values (from Rubin et al., 1985). (b) Mean bulk chemical composition of DIs in the four CO3 chondrites and bulk chemical compositions of Allende-AF and chondrule-like inclusions contained in Allende-AF (normalized to bulk Allende values) reported by Kojima and Tomeoka (1996).

5.3. Metamorphic Processes of the Host Meteorites

The four CO3 chondrites have experienced minor, various degrees of thermal metamorphism, ranging in petrologic type from 3.1 to 3.6, in their parent body (McSween, 1977a; Scott and Jones, 1990). It is important to clarify the relationship between the thermal metamorphism and the (earlier) secondary processes (aqueous alteration and subsequent dehydration) that have been experienced by DIs. Thermal metamorphism would equilibrate the FeO/(FeO + MgO) distribution of olivine in the meteorite matrices and at the same time decrease the bulk FeO/(FeO + MgO) ratio of matrix because of solid-state diffusive exchange between Fe-poor chondrules and Fe-rich matrix. Our defocused-beam analyses (Fig. 12) indicate that the DIs and the matrices were similarly affected by thermal metamorphism of the host meteorites. However, the degree of secondary alteration of DIs has no apparent correlation with the petrologic grades of the host meteorites, and there is no evidence of such secondary processes in the host meteorites. These observations suggest that the DIs were incorporated into the host meteorites before the thermal metamorphism took place. The secondary processes that affected the DIs were probably completed before incorporation, although the DIs experienced additional, minor metamorphism after incorporation. These interpretations are also consistent with the fact that the veins in the DIs, which resulted from aqueous alteration as we have argued above, terminate at the boundaries between DIs and the host meteorites.

5.4. CO Parent Body Implied by DIs

It was once widely thought that both CO3 and CV3 chondrites escaped any major degree of parent-body processing and thus preserve the most primitive state of parent bodies after accretion (e.g., McSween, 1979). In the case of the CV3 chondrites, however, much evidence of parent-body aqueous alteration has been revealed, in addition to the evidence from DIs (e.g., Tomeoka and Buseck, 1982a, 1982b, 1990; Keller et al., 1994; Lee et al., 1996; Brearley, 1997; Tomeoka and Tanimura, 2000). In contrast, for the CO3 chondrites, there are few data and limited evidence of secondary parent-body processes except the minor degree of thermal metamorphism discussed above. Although evidence for aqueous alteration (Kerridge, 1964; Ikeda, 1983; Keck and Sears, 1987; Keller and Buseck, 1990; Brearley, 1993; Rubin, 1998) and Na metasomatism in CAIs (Tomeoka et al., 1992; Kojima et al., 1995; Russell et al., 1998) has been reported from CO3 chondrites, the extent of those processes is apparently very minor relative to that in CV3 chondrites. In addition, unlike other types of chondrites, lithic clasts have rarely been reported from CO3 chondrites apart from occasional fragments of chondrules and CAIs (McSween, 1977a; Bunch and Rajan, 1988), which is usually taken to imply that brecciation was not active in the CO parent body. Consequently, the current consensus appears to be that the CO parent body was static and almost free of extensive aqueous alteration, thermal metamorphism, and brecciation.

Our study has revealed that DIs in the CO3 chondrites are probably clasts that have undergone aqueous alteration and dehydration at a location different from the location at which the host meteorite was lithified. An important question is what the precursors of the DIs are. The DIs are generally too small to compare their diagnostic petrographic features, such as chondrule size distribution, chondrule-to-matrix ratio, CAI abundance, and so on, with those of the host and other meteorites. Oxygen isotopic and trace element compositions of the DIs are currently unavailable. With these reservations, we suggest that the precursor of the DIs is probably CO chondrite material. The following data support this view: (1) The major element compositions and mineralogy of the DIs are similar to those of the Allende-AF DI (Fig. 11b), which is most likely to have been produced from the host Allende CV3 chondrite (Kojima and Tomeoka, 1996). Because CO3 and CV3 chondrites are similar in bulk chemical composition and mineralogy, the similarities suggest a genetic relationship between the DIs and their host CO3 chondrites. (2) The mineral species and compositions of Fe-Ni metal, including Co and Cr contents, in the DIs in all the

Table 5. Wavelength-dispensive X-ray spectrometry defocused-beam (30 μm in diameter) analyses of dark inclusions (DIs) and matrices in the four CO3 chondrites.

	Kainsaz (3.1)				Ornans (3.3)				Lancé (3.4)				Warrenton (3.6)			
	DIs		Matrix		DIs		Matrix		DIs		Matrix		DIs		Matrix	
N_1	21				23				19				13			
N_2	65		117		116		55		113		72		47		50	
		(SD)		(SD)		(SD)		(SD)		(SD)		(SD)		(SD)		(SD)
Na_2O	0.76	0.33	0.73	0.25	0.52	0.32	0.35	0.40	0.51	0.36	0.37	0.16	0.40	0.27	0.31	0.19
Al_2O_3	1.85	0.79	2.46	0.69	1.95	0.93	2.87	0.87	2.12	0.87	2.50	0.89	3.95	1.32	4.83	1.15
K_2O	0.20	0.07	0.21	0.08	0.17	0.08	0.13	0.05	0.18	0.04	0.14	0.03	0.12	0.03	0.11	0.03
TiO_2	0.29	0.06	0.33	0.03	0.31	0.13	0.33	0.03	0.35	0.05	0.35	0.03	0.32	0.05	0.33	0.03
FeO	38.4	7.43	30.6	5.04	31.2	3.92	29.5	3.09	31.1	2.43	30.6	4.36	26.6	3.65	23.5	2.65
MgO	13.9	3.71	17.6	2.65	18.1	2.04	16.3	1.80	18.8	1.35	19.9	1.99	22.5	2.25	19.9	1.80
SiO_2	27.7	3.17	30.3	2.19	29.1	3.75	25.4	2.26	30.3	2.16	28.1	2.08	29.9	3.51	25.6	2.35
CaO	1.36	0.83	1.09	1.39	1.08	0.77	0.61	0.37	0.86	0.51	0.63	1.41	0.89	1.67	0.52	0.99
MnO	0.88	0.17	0.88	0.11	0.69	0.13	0.72	0.06	0.67	0.07	0.79	0.05	0.75	0.06	0.68	0.05
P_2O_5	0.21	0.15	0.29	0.07	0.57	0.41	0.18	0.09	0.17	0.11	0.22	0.22	0.24	0.12	0.20	0.05
NiO	0.96	0.55	0.82	0.47	0.54	0.44	0.73	0.53	0.50	0.43	0.72	0.49	0.39	0.25	0.60	0.52
Cr_2O_3	0.35	0.29	0.51	0.07	0.47	0.20	0.49	0.15	0.58	0.23	0.56	0.27	0.73	0.58	0.65	0.18
S	1.21	0.85	0.75	0.35	0.98	0.32	0.64	0.29	1.06	0.25	0.74	0.31	0.96	0.26	0.55	0.32
Total	88.1		86.5		85.7		78.2		87.1		85.6		87.7		77.8	
FM ratio	0.73		0.63		0.63		0.64		0.62		0.61		0.54		0.54	
Elemental abundances normalized to Si (Si = 1; atomic ratios)																
Na	0.044		0.038		0.028		0.022		0.027		0.021		0.021		0.019	
Al	0.076		0.092		0.076		0.128		0.079		0.101		0.149		0.214	
K	0.013		0.012		0.010		0.009		0.010		0.009		0.007		0.008	
Ti	0.013		0.014		0.014		0.016		0.015		0.016		0.014		0.017	
Fe	2.31		1.68		1.78		1.93		1.71		1.81		1.48		1.53	
Mg	0.647		0.749		0.802		0.828		0.800		0.913		0.971		1.00	
Ca	0.075		0.055		0.057		0.037		0.043		0.034		0.045		0.031	
Mn	0.053		0.048		0.039		0.047		0.036		0.047		0.041		0.044	
P	0.007		0.009		0.018		0.007		0.005		0.007		0.008		0.007	
Ni	0.058		0.045		0.031		0.048		0.028		0.043		0.022		0.039	
Cr	0.018		0.024		0.024		0.028		0.028		0.029		0.036		0.037	
S	0.093		0.053		0.072		0.054		0.075		0.056		0.069		0.046	

N_1 = number of DIs, N_2 = number of analyses, FM ratio = FeO/(MgO + FeO) weight ratio.

four CO3 chondrites are virtually identical to those of their own host chondrites (Table 4). We believe that this fact in particular places a strong constraint against the possibility of a CV3 chondrite as a precursor of the CO3 DIs because metal mineralogy and compositions are distinctly different between CV3 and CO3 chondrites (McSween, 1977a, 1977b). (3) The DIs have very similar abundances in all the four CO3 chondrites (Table 2). We believe that this similarity weakens the possibility that the DIs are fragments of a foreign parent body that were introduced by meteorite infall. Rather, it suggests that the brecciation event that dispersed DI fragments to the four CO3 chondrites took place on their own host parent body.

Another important implication derived from the results of our study is that the CO3 chondrites may have undergone considerably more brecciation in their parent body than has previously been recognized. Compared to CV3 DIs, CO3 DIs show the following major differences: They are much smaller in size, more rounded in shape, and much higher in number density in the host meteorites. Assuming that these processes that produced these characteristics occurred in the CO parent body, the differences suggest that the fragmentation of the parent rock of the DIs in the CO parent body was thorough and extensive. Thus, more abundant and smaller fragments were generated than in the CV parent body. Individual fragments may have been rounded by abrasion during brecciation and transportation. As already noted, the DIs were incorporated into the host meteorites before the thermal metamorphism of the host meteorites started. Therefore, the brecciation process may have occurred before the thermal metamorphism of the host meteorites. Because the CO3 chondrites do not appear to contain clasts of different petrologic types within the same chondrite, no significant brecciation may have occurred after the thermal metamorphism started. We envisage that all these processes occurred near the outer regolith of the CO parent body, where impact brecciation would have been most effective.

Taking these considerations into account, it is conceivable that the CO parent body has not escaped major physical and chemical processing since accretion, as implicitly imagined previously. Rather, it is likely that the CO parent body contained water heterogeneously, and as it was heated, aqueous alteration occurred extensively in the regions where water existed. However, as the water was lost and/or consumed, those regions may have been dehydrated with continuous heating. Brecciation processes including fragmentation, transportation and reincorporation may also have occurred actively in the CO parent body. The host CO3 chondrites perhaps represent a relatively dry unaltered region in the parent body, whereas DIs came from a formerly wet, highly altered region.

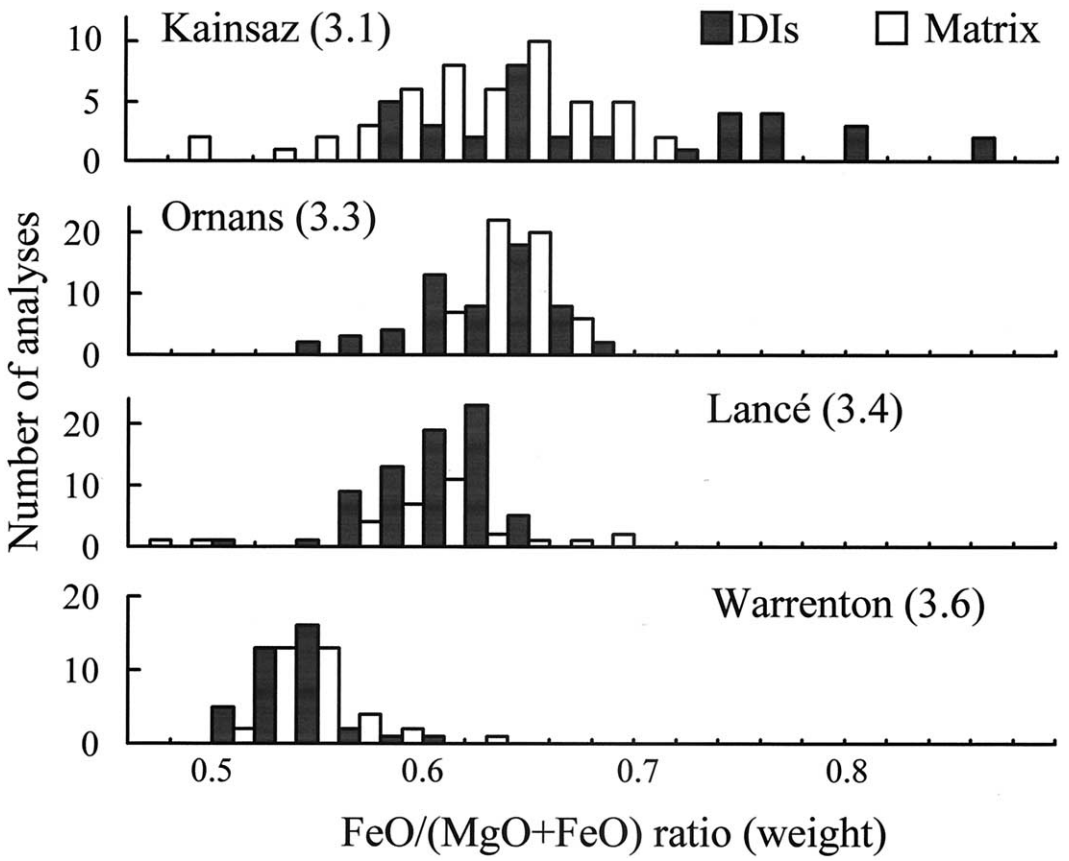

Fig. 12. Spatial distributions of FeO/(FeO + MgO) weight ratios in dark inclusions (DIs) and the matrices in the four CO3 chondrites. The wavelength-dispersive X-ray spectrometry analysis was performed at the density of one analysis/100 × 100 μm area, using a 30-μm diameter beam; areas including opaque mineral grains > 5 μm in diameter were avoided.

6. CONCLUSIONS

1. Our study has revealed that DIs occur at the ~1-vol.% level in the four CO3 chondrites Kainsaz, Ornans, Lancé, and Warrenton. This indicates that DIs are important constituents of the meteorites. Most DIs are rounded in shape and smaller in size than those in CV3 chondrites. The DIs consist mainly of fine grains of Fe-rich olivine, and on the basis of texture, they can be divided into two types. Type I DIs contain rounded to oval-shaped objects that are aggregates of fine grains in a fine-grained matrix, resembling chondrule-like inclusions in type B DIs in CV3 chondrites. Type II DIs lack rounded objects and are almost featureless in texture, resembling type C DIs in CV3 chondrites. Olivine grains of both type I DIs and type II DIs contain numerous microinclusions of Fe-Ni metal and troilite and microcavities, which also resemble those in DIs in CV3 chondrites. Bulk major element compositions of the DIs are similar to that of an Allende DI (Allende-AF).
2. The DIs probably have experienced aqueous alteration and subsequent dehydration on the meteorite parent body and thus have a formation history similar to that of DIs in CV3 chondrites. Our observations suggest that type I DIs are fragments of chondrule pseudomorphs. The rounded objects in type I DIs were probably formed by replacing phenocrysts of olivine and enstatite in chondrules. Type I DIs contain networks of veins filled with Fe-rich olivine, which is another characteristic that they have in common with DIs in CV3 chondrites and which provides strong evidence that the DIs have been involved in aqueous alteration. Type II DIs may have resulted from size sorting and reassembly of fine grains that had been disaggregated from a type I DI rock.
3. From the major element compositions, the mineralogy of metallic phases, and the widely dispersed nature of the DIs, we suggest that the precursor of the DIs was CO chondrite material. In particular, the DIs are probably clasts of the CO parent body that have experienced aqueous alteration and subsequent dehydration at a location different from the location from which the host meteorites came. We infer that the CO parent body was a heterogeneous conglomerate consisting of water-bearing regions and water-free regions and that during asteroidal heating, the water-bearing regions were aqueously altered and subsequently dehydrated. Our inference that the DIs were transported from one location to another may also imply that brecciation processes including fragmentation, transportation, and reincorporation occurred actively in the CO parent body.
4. The distribution of FeO/(FeO + MgO) ratios in the DIs and the matrices in the host meteorites indicate that the DIs and the matrices were similarly affected by thermal metamorphism of the host meteorites (petrologic grades 3.1 to 3.6).

However, the degree of secondary processing (aqueous alteration and subsequent dehydration) of the DIs has no apparent correlation with the petrologic grades of the host meteorites. These observations suggest that the DIs were incorporated into the host meteorites before the thermal metamorphism took place and that the secondary processes of the DIs were largely completed before incorporation into the present location.

Acknowledgments—We thank Dr. G. MacPherson for providing Kainsaz and Ornans samples and Dr. G. Kurat for providing Lancé and Warrenton samples. This paper has greatly benefited from thorough reviews by Drs. A. Brearley, G. Herzog, and L. Keller as well as an anonymous reviewer. Electron microprobe analysis was performed at the Venture Business Laboratory, Kobe University. This work was supported by Grant-in-Aid of the Japan Ministry of Educations, Science and Culture (no. 09440187).

Associate editor: G. F. Herzog

REFERENCES

Brearley A. J. (1993) Matrix and fine-grained rims in the unequilibrated CO3 chondrite, ALHA77307: Origins and evidence for diverse, primitive nebular dust components. *Geochim. Cosmochim. Acta* **57,** 1521–1550.

Brearley A. J. (1997) Disordered biopyriboles, amphibole, and talc in the Allende meteorite: Products of nebular or parent body aqueous alteration? *Science* **276,** 1103–1105.

Brearley A. J. and Prinz M. (1996) Dark inclusions in the Allende meteorite: New insights from transmission electron microscopy [abstract]. *Lunar Planet. Sci.* **27,** 161–162.

Brearley A. J. and Jones R. H. (1998) Chondritic meteorites. *Rev. Mineral.* **36,** 3-1–3-398.

Buchanan P. C., Zolensky M. E., and Reid A. M. (1997) Petrology of Allende dark inclusions. *Geochim. Cosmochim. Acta* **61,** 1733–1743.

Bunch T. E. and Rajan R. S. (1988) Meteorite regolithic breccias. In *Meteorites and the Early Solar System* (eds. J. F. Kerridge and M. S. Matthews), pp. 144–164. Tucson: University of Arizona Press.

Bunch T. E., Chang S., and Ott U. (1980) Regolith origin for Allende meteorite. *Lunar Planet. Sci.* **11,** 119–121.

Fruland R. M., King E. A., and McKay D. S. (1978) Allende dark inclusions. In *Proc. Lunar Planet. Sci. Conf. 9th*, pp. 1305–1329.

Ikeda Y. (1983) Alteration of chondrules and matrices in the four Antarctic carbonaceous chondrites ALH-77307(C3), Y-790123(C2), Y-75293(C2), and Y-74662(C2). *Mem. Natl. Inst. Polar Res.* **30,** 93–108.

Johnson C. A., Prinz M., Weisberg M. K., Clayton R. N., and Mayeda T. K. (1990) Dark inclusions in Allende, Leoville, and Vigarano: Evidence for nebular oxidation of CV3 constituents. *Geochim. Cosmochim. Acta* **54,** 819–830.

Keck B. D. and Sears D. W. G. (1987) Chemical and physical studies of type 3 chondrites-VIII: Thermoluminescence and metamorphism in the CO chondrites. *Geochim. Cosmochim. Acta* **51,** 3013–3021.

Keller L. P. and Buseck P. R. (1990) Matrix mineralogy of the Lancé CO3 carbonaceous chondrite: A transmission electron microscope study. *Geochim. Cosmochim. Acta* **54,** 1155–1163.

Keller L. P., Thomas K. L., Clayton R. N., Mayeda T. K., DeHart J. M., and McKay D. S. (1994) Aqueous alteration of the Bali CV3 chondrite: Evidence from mineralogy, mineral chemistry, and oxygen isotopic compositions. *Geochim. Cosmochim. Acta* **58,** 5589–5598.

Kerridge J. F. (1964) Low-temperature minerals from the fine-grained matrix of some carbonaceous chondrites. *Ann. N. Y. Acad. Sci.* **119,** 41–53.

Kojima T. and Tomeoka K. (1996) Indicators of aqueous alteration and thermal metamorphism on the CV parent body: Microtextures of a dark inclusion from Allende. *Geochim. Cosmochim. Acta* **60,** 2651–2666.

Kojima T., Tomeoka K., and Takeda H. (1993) Unusual dark clasts in the Vigarano CV3 carbonaceous chondrite: Record of parent body process. *Meteoritics* **28,** 649–658.

Kojima T., Yada S., and Tomeoka K. (1995) Ca-Al-rich inclusions in three Antarctic CO3 chondrites, Yamato-81020, Yamato-82050 and Yamato-790992: Record of low temperature alteration processes. *Proc. NIPR Symp. Antarct. Meteorites* **8,** 79–96.

Krot A. N., Scott E. R. D., and Zolensky M. E. (1995) Mineralogical and chemical modification of components in CV3 chondrites: Nebular or asteroidal processing? *Meteoritics* **30,** 748–775.

Krot A. N., Scott E. R. D., and Zolensky M. E. (1997) Origin of fayalitic olivine rims and lath-shaped matrix olivine in the CV3 chondrite Allende and its dark inclusions. *Meteorit. Planet. Sci.* **32,** 31–49.

Krot A. N., Petaev M. I., Zolensky M. E., Keil K., Scott E. R. D., and Nakamura K. (1998) Secondary calcium-iron-rich minerals in the Bali-like and Allende-like oxidized CV3 chondrites and Allende dark inclusions. *Meteorit. Planet. Sci.* **33,** 623–645.

Krot A. N., Brearley A. J., Ulyanov A. A., Biryukov V. V., Swindle T. D., Keil K., Mittlefehldt D. W., Scott E. R. D., Clayton R. N., and Mayeda T. K. (1999) Mineralogy, petrography, bulk chemical, iodine-xenon, and oxygen-isotopic compositions of dark inclusions in the reduced CV3 chondrite Efremovka. *Meteorit. Planet. Sci.* **34,** 67–89.

Kurat G., Palme H., Brandstätter F., and Huth J. (1989) Allende Xenolith AF: Undisturbed record of condensation and aggregation of matter in the solar nebula. *Z. Naturforsch.* **44a,** 988–1004.

Lee M. R., Hutchison R., and Graham A. L. (1996) Aqueous alteration in the matrix of the Vigarano (CV3) carbonaceous chondrite. *Meteorit. Planet. Sci.* **31,** 477–483.

McSween H. Y., Jr. (1977a) Carbonaceous chondrites of the Ornans type: A metamorphic sequence. *Geochim. Cosmochim. Acta* **41,** 477–491.

McSween H. Y., Jr. (1977b) Petrographic variations among carbonaceous chondrites of the Vigarano type. *Geochim. Cosmochim. Acta* **41,** 1777–1790.

McSween H. Y., Jr. (1979) Are carbonaceous chondrites primitive or processed? A review. *Rev. Geophys. Space Phys* **17,** 1059–1078.

Palme H., Kurat G., Spettel B., and Burghele A. (1989) Chemical composition of an unusual xenolith of the Allende meteorite. *Z. Naturforsch.*, **44a:** 1005–1014.

Richardson S. M. (1978) Vein formation in the C1 carbonaceous chondrites. *Meteoritics* **13,** 141–159.

Rubin A. E. (1998) Correlated petrologic and geochemical characteristics of CO3 chondrites. *Meteorit. Planet. Sci.* **33,** 385–391.

Rubin A. E., James J. A., Keck B. D., Weeks K. S., Sears D. W. G., and Jarosewich E. (1985) The Colony meteorite and variations in CO3 chondrite properties. *Meteoritics* **20,** 175–196.

Russell S. S., Huss G. R., Fahey A. J., Greenwood R. C., Hutchison R., and Wasserburg G. J. (1998) An isotopic and petrologic study of calcium-aluminum-rich inclusions from CO3 meteorites. *Geochim. Cosmochim. Acta* **62,** 689–714.

Scott E. R. D. and Jones R. H. (1990) Disentangling nebular and asteroidal features of CO3 carbonaceous chondrite meteorites. *Geochim. Cosmochim. Acta* **54,** 2485–2502.

Tomeoka K. (1990) Phyllosilicate veins in a CI meteorite: Evidence for aqueous alteration on the parent body. *Nature* **345,** 138–140.

Tomeoka K. and Buseck P. R. (1982a) Intergrown mica and montmorillonite in the Allende carbonaceous chondrite. *Nature* **299,** 326–327.

Tomeoka K. and Buseck P. R. (1982b) An unusual layered mineral in chondrules and aggregates of the Allende carbonaceous chondrite. *Nature* **299,** 327–329.

Tomeoka K. and Buseck P. R. (1990) Phyllosilicates in the Mokoia CV carbonaceous chondrite: Evidence for aqueous alteration in an oxidizing condition. *Geochim. Cosmochim. Acta* **54,** 1745–1754.

Tomeoka K. and Kojima T. (1998) Arcuate band texture in a dark inclusion from the Vigarano CV3 chondrite: Possible evidence for early sedimentary processes. *Meteorit. Planet. Sci.* **33,** 519–525.

Tomeoka K. and Tanimura I. (2000) Phyllosilicate-rich chondrule rims in the Vigarano CV3 chondrite: Evidence for parent-body processes. *Geochim. Cosmochim. Acta* **64,** 1971–1988.

Tomeoka K., Nomura K., and Takeda H. (1992) Na-bearing Ca-Al-rich inclusions in the Yamato-791717 CO carbonaceous chondrite. *Meteoritics* **27,** 136–143.

Weisberg M. K. and Prinz M. (1998) Fayalitic olivine in CV3 chondrite matrix and dark inclusions: A nebular origin. *Meteorit. Planet. Sci.* **33,** 1087–1099.